2013 IEEE/RSJ International Conference on
Intelligent Robots and Systems (IROS)
November 3-7, 2013. Tokyo, Japan

Magnetotactic Bacteria and Microjets: A Comparative Study

Islam S. M. Khalil*♭, Veronika Magdanz†, Samuel Sanchez†, Oliver G. Schmidt†‡, and Sarthak Misra*
*University of Twente, Enschede, The Netherlands
♭German University in Cairo, New Cairo City, Egypt
†Institute for Integrative Nanosciences, IFW Dresden, Germany
‡Material Systems for Nanoelectronics, University of Technology Chemnitz, Germany

***Abstract*— We provide a comparative study between two self-propelled microrobots, i.e., magnetotactic bacteria and microjets. This study includes characterization of their fluidic properties (linear and rotational drag coefficients) based on their morphologies and characterization of their magnetic properties using the *rotating-field* technique. Further, the control characteristics of our microrobots are evaluated in the transient- and steady-states. The average boundary frequencies of our magnetotactic bacteria and microjets are 2.2 rad/s and 25.1 rad/s, respectively. The characterized fluidic properties and boundary frequencies are used in the characterization of the magnetic properties of our microrobots. The average magnetic dipole moments of our magnetotactic bacteria and microjets are 1.4×10^{-17} A.m^2 and 1.5×10^{-13} A.m^2 at magnetic field of 2 mT and linear velocities of 32 μm/s (approximately 6 body lengths per second) and 119 μm/s (approximately 2 body lengths per second), respectively. These characterized magnetic dipole moments are utilized in the realization of closed-loop control systems for the magnetotactic bacteria and microjets. Our closed-loop control system positions the magnetotactic bacteria and the microjets within the vicinity of reference positions with average diameters of 23 μm (approximately 4 body lengths) and 417 μm (approximately 8 body lengths), respectively.**

I. INTRODUCTION

Self-propelled magnetic microrobots [1]-[5] benefit from the larger projection distance of the magnetic fields, as opposed to magnetic microrobots that are steered by the magnetic field gradients [6], [7]. These microrobots, i.e., magnetotactic bacteria and microjets (Fig. 1), have the potential to execute non-trivial tasks, such as microassembly [8], [9], micromanipulation [10] and microactuation [11], under the influence of the controlled magnetic fields.

Martel *et al*. used *Magnetospirillum gryphiswaldense* magnetotactic bacteria to manipulate a 3 μm bead at an average velocity of 7.5 μm/s [12]. Kim *et al.* also demonstrated the three-dimensional control of *Tetrahymena Pyriformis* cells using two sets of Helmholtz coils and a single electromagnet to control the planar and vertical motion of these cells, respectively [13]. *Serratia marcescens* were integrated to a microstructure to provide propulsion by Sakar *et al.* [14]. Khalil *et al.* demonstrated the point-to-point motion control of a magnetotactic bacterium (MTB), i.e., *Magnetospirillum magnetotacticum* (MS-1) inside capillary tubes and fluidic microchannels [15].

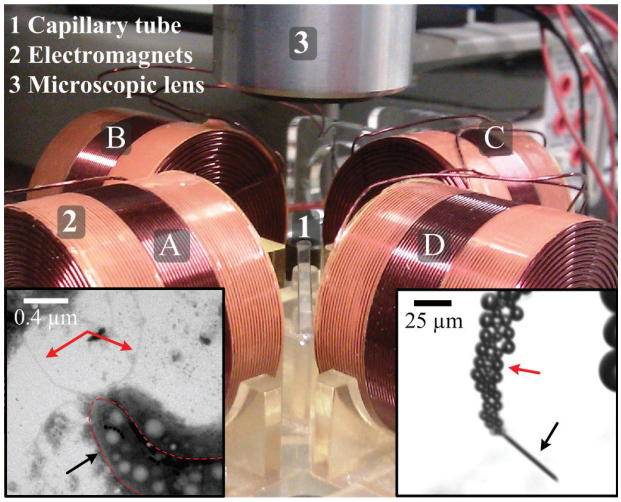

Fig. 1. Magnetic system for the wireless control of magnetotactic bacteria and self-propelled microjets. Magnetotactic bacteria are incubated and controlled inside a capillary tube with growth medium, whereas microjets are controlled inside a petri dish (not shown) with hydrogen peroxide solution. The magnetite nanocrystals of the magnetotactic bacteria and the magnetic layers of the microjets allow for their orientation along the external magnetic field lines. Magnetotactic bacteria move along the magnetic field lines using their flagella, shown by the red arrows at the bottom-left Scanning Electron Microscopy image. Microjets move along the magnetic field lines by the self-propulsion force due to the ejecting oxygen bubbles (indicated by the red arrow in the bottom-right microscopic image) generated by the catalytic decomposition of the hydrogen peroxide solution.

The aforementioned microrobots provide self-propulsion by their flagella or cilia, whereas microjets provide propulsion by the conversion of the chemical energy to kinetic energy through a catalytic reaction between their tubular layers and the surrounding solution [9], [16]. Sanchez *et al.* demonstrated the magnetic-based control of microjets inside the channels of a microfluidic system against the flow of a hydrogen peroxide solution [17]. It has been also shown that self-propelled microjets can selectively transport large amounts of particles on chip [9] and Murine Cath.a-differentiated cells by controlling the magnetic fields [10].

In this work, we provide a comparative study between two self-propelled microrobots, i.e., magnetotactic bacteria and microjets. This comparative study is achieved by characterizing the fluidic, magnetic and control properties

*Islam S. M. Khalil and Sarthak Misra are affiliated with MIRA–Institute for Biomedical Technology and Technical Medicine, University of Twente.

†Veronika Magdanz, Samuel Sanchez and Oliver G. Schmidt thank the Volkswagen Foundation (# 86 362). The research leading to these results has received funding from the European Research Council under the European Union's Seventh Framework Programme (FP7/2007-2013) / ERC grant agreement n° 311529.

of each microrobot. The fluidic properties are calculated based on the morphologies of the microrobots. The magnetic characterization includes the determination of the boundary frequencies and the magnetic dipole moments of our microrobots, whereas the control characteristics are determined by analyzing the transient- and steady-state control characteristics of each microrobot. The boundary frequencies and magnetic dipole moments are determined by applying rotating magnetic fields at gradually increasing frequencies that range from 1 rad/s to 100 rad/s. At the boundary frequencies, the microrobots can no longer follow the rotating fields. The characterized boundary frequencies and magnetic dipole moments are used in the realization of the magnetic force-current maps for our magnetic system. The closed-loop control system is designed based on these maps.

The remainder of this paper is organized as follows: Section II provides a comparison between the fluidic and magnetic properties of magnetotactic bacteria and microjets. These properties are determined based on the characterized morphologies, and by applying rotating magnetic fields to determine the boundary frequencies and magnetic dipole moments of the microrobots. In Section III, we use the characterized magnetic dipole moments to design closed-loop control systems. These systems are used to achieve point-to-point positioning of the microrobots. Finally, Section IV concludes and provides directions for future work.

II. CHARACTERIZATION COMPARISON

Magnetotactic bacteria and microjets move in a growth medium [18] and hydrogen peroxide solution, respectively. Magnetotactic bacteria align themselves along the external magnetic field lines using the magnetite nanocrystals enveloped in their membranes (Fig. 2), whereas microjets align themselves using the iron layer of their tubular structure. Magnetotactic bacteria provide propulsion force by rotating their flagella, while microjets provide propulsion by the ejecting oxygen bubbles due to the catalytic decomposition of the hydrogen peroxide solution. Therefore, these self-propelled microrobots experience magnetic and drag forces and torques, and self-propulsion forces and torques.

A. Modeling of Self-Propelled Microrobots

In a low Reynolds number regime, motion of our self-propelled microrobots is governed by

$$\mid \mathbf{F}(\mathbf{P}) \mid + F_{\mathrm{d}} + f = 0 \quad \text{and} \quad \mid \mathbf{T}(\mathbf{P}) \mid + T_{\mathrm{d}} + \Gamma = 0, \quad (1)$$

where $\mathbf{F}(\mathbf{P}) \in \mathbb{R}^{3\times 1}$ and $\mathbf{T}(\mathbf{P}) \in \mathbb{R}^{3\times 1}$ are the magnetic force and torque experienced by our microrobots at position $\left(\mathbf{P} \in \mathbb{R}^{3\times 1}\right)$, respectively. Further, F_{d} and T_{d} are the drag force and torque, respectively. The drag force and torque depend linearly on the linear and angular velocities of our microrobots. In (1), f and Γ are the self-propulsion force and torque, respectively. The magnetic force and torque are given by

$$\mathbf{F}(\mathbf{P}) = (\mathbf{m}\cdot\nabla)\mathbf{B}(\mathbf{P}) \quad \text{and} \quad \mathbf{T}(\mathbf{P}) = \mathbf{m}\times\mathbf{B}(\mathbf{P}). \quad (2)$$

In (2), $\mathbf{m} \in \mathbb{R}^{3\times 1}$ and $\mathbf{B}(\mathbf{P}) \in \mathbb{R}^{3\times 1}$ are the magnetic dipole moment of the microrobots and the induced magnetic field,

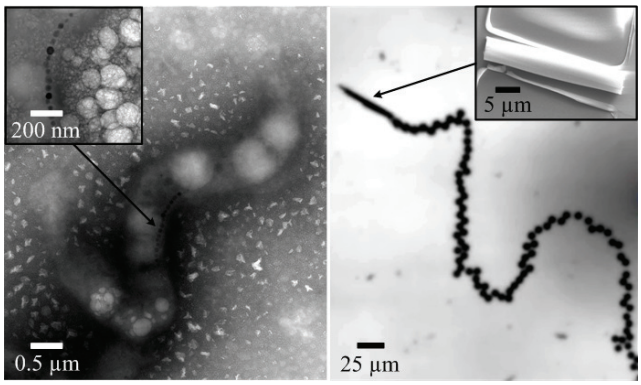

Fig. 2. Self-propelled microrobots are controlled under the influence of the magnetic fields. Left: Scanning Electron Microscopy (SEM) image of a magnetotactic bacterium (MTB), i.e., Strain *Magnetospirillum magnetotacticum* MS-1. The membrane of the MTB envelopes magnetite nanocrystals, shown by the Transmission Electron Microscopy image in the inset. These nanocrystals allow the MTB to align itself along the external magnetic field lines. An MTB moves along the field lines by rotating its flagella (not shown). Right: Microscopic image of a self-propelled microjet. The nickel and iron tubular layers of the microjet allow for its orientation along the external magnetic field lines. Self-propulsion of the microjet is achieved using the ejecting oxygen bubbles from its end due to the catalytic decomposition of the hydrogen peroxide solution. The inset shows a SEM image of a fixed microjet to the substrate.

respectively. The magnetic torque aligns our microrobots along the magnetic field lines, then their propulsion forces allow them to move. The drag forces $(\mathbf{F}_{\mathrm{d}}(\dot{\mathbf{P}}) \in \mathbb{R}^{3\times 1})$ and torques $(\mathbf{T}_{\mathrm{d}}(\mathbf{\Omega}) \in \mathbb{R}^{3\times 1})$ are given by

$$\mathbf{F}_{\mathrm{d}}(\dot{\mathbf{P}}) = \gamma\dot{\mathbf{P}} \quad \text{and} \quad \mathbf{T}_{\mathrm{d}}(\mathbf{\Omega}) = \alpha\mathbf{\Omega}, \quad (3)$$

where $\dot{\mathbf{P}} \in \mathbb{R}^{3\times 1}$ and $\mathbf{\Omega} \in \mathbb{R}^{3\times 1}$ are the linear and angular velocities of the microrobots, respectively. Further, γ is the linear drag coefficient and is given by [19]

$$\gamma = 2\pi\eta l\left[\ln\left(\frac{2l}{d}\right) - 0.5\right]^{-1}, \quad (4)$$

where l and d are the length and diameter of an MTB or a microjet, respectively. Further, η is the dynamic viscosity of the fluid that is assumed to have the same dynamic viscosity as water ($\eta = 1$ mPa.s). In (3), α is the rotational drag coefficient and is given by [20]

$$\alpha = \frac{\pi\eta l^3}{3}\left[\ln\left(\frac{l}{d}\right) + 0.92\left(\frac{d}{l}\right) - 0.662\right]^{-1}. \quad (5)$$

The linear and rotational drag coefficients have to be calculated to determine the drag forces and torques experienced by the microrobots.

B. Characterization of Fluidic Properties: Drag Coefficients

The linear and rotational drag coefficients are calculated using (4) and (5), respectively. This calculation is based on the characterized morphologies of magnetotactic bacteria and microjets. The morphology of the magnetotactic bacteria is determined from 15 Scanning/Transmission Electron Microscopy (SEM/TEM) images, whereas the morphology of microjets is derived from a single SEM image. The average length (l) and average diameter (d) of magnetotactic bacteria

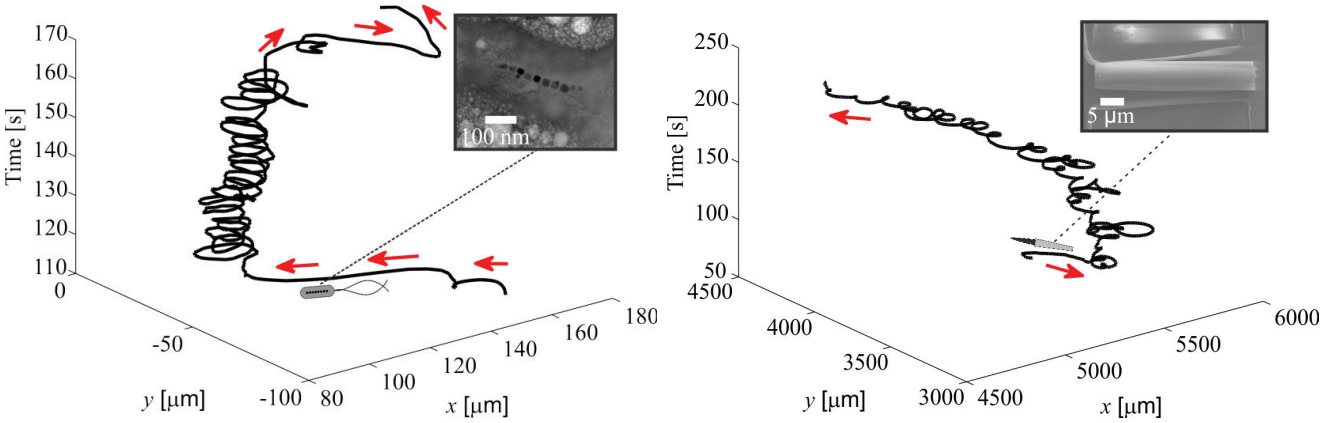

(a) Magnetotactic bacterium undergoes circular trajectories

(b) Microjet undergoes circular trajectories

Fig. 3. Characterization of the magnetic dipole moment of the self-propelled microrobots using the *rotating field* technique [4]. Rotating magnetic fields are applied using our magnetic system and the boundary frequencies of the microrobots are determined from their motion analysis. The magnetic dipole moment is calculated using (7). The red arrows indicate the direction of the microrobots. The characterized magnetic dipole moments are used in the realization of the magnetic force-current map of our system. (a) Magnetotactic bacterium (MTB) undergoes circular trajectories under the influence of the rotating magnetic fields. We observe that the boundary frequency is 2.2 rad/s, at magnetic field of 2 mT. The average magnetic dipole moment of our magnetotactic bacteria is 1.4×10^{-17} A.m^2. The inset shows a Transmission Electron Microscopy image of the magnetite nanocrystals enveloped in the membrane of an MTB that uses these nanocrystals to align along the rotating field lines. (b) Microjet undergoes circular trajectories under the influence of the rotating magnetic fields. We observe that the boundary frequency is 25.1 rad/s, at magnetic field of 2 mT. The average magnetic dipole moment of our microjets is 1.5×10^{-13} A.m^2. The inset shows a Scanning Electron Microscopy image of a microjet fixed to its substrate.

are calculated to be 5.2 μm and 0.5 μm, respectively. The length and outer diameter of the microjet are 50 μm and 5 μm, respectively. Using the characterized morphologies of the microrobots and (4), the linear drag coefficients of magnetotactic bacteria and microjets are 1.2×10^{-8} N.m^{-1}.s and 1.2×10^{-7} N.m^{-1}.s, respectively. Using (5), the rotational drag coefficients of our magnetotactic bacteria and microjets are 8.3×10^{-20} N.m.s and 7.5×10^{-17} N.m.s, respectively. These coefficients along with the characterized boundary frequencies are used to determine the magnetic dipole moments of our microrobots.

C. Characterization of Magnetic Properties

1) Boundary Frequency: The self-propelled microrobots undergo circular trajectories under the influence of rotating magnetic fields, as shown in Fig. 3. Increasing the frequency of the rotating fields increases the angular velocities of the microrobots. The relation between the magnetic torque and the angular velocity of the microrobot ($\mathbf{\Omega}$) is given by

$$\mid \mathbf{m} \mid\mid \mathbf{B}(\mathbf{P}) \mid \sin\beta + \alpha \mid \mathbf{\Omega} \mid = 0, \tag{6}$$

where β is the angle between the induced magnetic field and the magnetic dipole moment of the microrobot. Characterization of the magnetic dipole moment requires the determination of its boundary frequency (ω_b). This frequency can be determined by gradually increasing the frequency of the rotating field and observing the frequency after which an MTB or a microjet can no longer follow the rotating magnetic fields, i.e., $\mid \mathbf{\Omega} \mid = \omega_\mathrm{b}$, when $\sin\beta = 1$. Therefore, (6) can be written as

$$\mid \mathbf{m} \mid\mid \mathbf{B}(\mathbf{P}) \mid + \alpha\omega_\mathrm{b} = 0. \tag{7}$$

Rotating magnetic fields are generated using our magnetic system (Fig. 1). The frequencies of these fields are increased from 1 rad/s to 100 rad/s to observe the boundary frequency of our microrobots. Fig. 3(a) shows a representative *rotating field* characterization experiment of an MTB. We repeated this experiment 10 times and the average boundary frequency is calculated to be 2.2 rad/s, at magnetic field of 2 mT. Similarly, Fig. 3(b) provides a representative *rotating field* characterization experiment of a microjet. The average boundary frequency is 25.1 rad/s, at magnetic field of 2 mT.

2) Magnetic Dipole Moment: We use the characterized rotational drag coefficients and boundary frequencies of our self-propelled microrobots to determine the magnetic dipole moments using (7). The average magnetic dipole moments of the magnetotactic bacteria and microjets are calculated to be 1.4×10^{-17} A.m^2 and 1.5×10^{-13} A.m^2 at magnetic field of 2 mT, respectively. The averages are calculated from 10 characterization experiments for each microrobot. The characterized magnetic dipole moments are used in the realization of the magnetic force-current maps that are used in the implementation of the closed-loop control system.

III. CONTROL COMPARISON

Our control strategy is based on orienting the magnetic fields towards a reference position without controlling the magnetic torque. The magnetic field and the magnetic force field have the same direction and are almost identical within the workspace of our magnetic system. Therefore, controlling the field lines is achieved through the following magnetic force-current map [7], [15]:

$$\mathbf{F}(\mathbf{P}) = (\mathbf{m}(\mathbf{P}) \cdot \nabla)\widetilde{\mathbf{B}}(\mathbf{P})\mathbf{I} = \mathbf{\Lambda}(\mathbf{m}, \mathbf{P})\mathbf{I}, \tag{8}$$

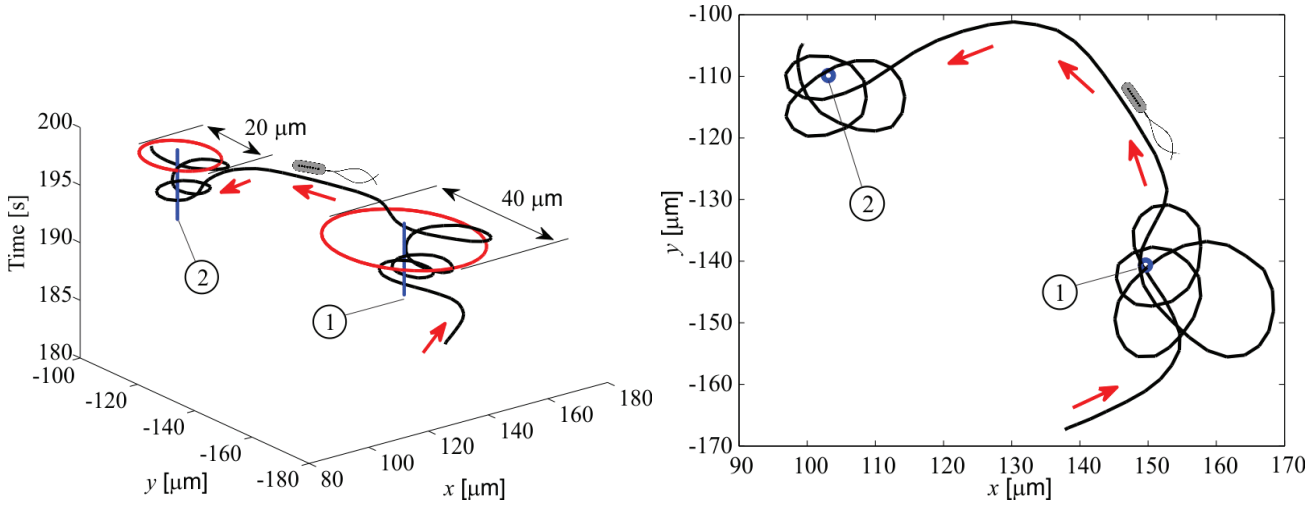

(a) Path of the controlled magnetotactic bacterium

(b) Controlled MTB within the vicinity of two reference positions

Fig. 4. Representative closed-loop motion control result of a magnetotactic bacterium (MTB), i.e., Strain *Magnetospirillum magnetotacticum* MS-1, under the influence of the controlled magnetic fields. Our MTB is positioned within the vicinity of two reference positions using control law (9). The entries of the diagonal matrices $\mathbf{K}_\mathrm{p}$ and $\mathbf{K}_\mathrm{d}$ are 15 s^{-2} and 15.5 s^{-1}, respectively. (a) An MTB is controlled at an average velocity of 30 μm/s. The control system positions the MTB within the vicinity of two reference positions (vertical blue lines) with regions of convergence of 40 μm and 20 μm in diameter. (b) The control system reverses the direction of the magnetic fields to position the MTB within the vicinity of the reference positions (blue circles), based on (11). *Please refer to the attached video that demonstrates the results of the closed-loop control of an MTB.*

where $\widetilde{\mathbf{B}}(\mathbf{P}) \in \mathbb{R}^{3\times n}$ is a matrix that maps the current vector ($\mathbf{I} \in \mathbb{R}^{3\times 1}$) into magnetic fields ($\mathbf{B}(\mathbf{P})$). Further, $\mathbf{\Lambda}(\mathbf{m},\mathbf{P}) \in \mathbb{R}^{3\times n}$ is the actuation matrix that can be evaluated based on the dipole moment of each of the microrobots [7]. The pseudoinverse of the actuation matrix is evaluated for the implementation of the closed-loop control to calculate the currents at each of the electromagnets based on the desired magnetic force. We devise the following controlled magnetic force to orient the magnetic field lines towards a reference position ($\mathbf{P}_\mathrm{ref} \in \mathbb{R}^{3\times 1}$):

$$\mathbf{F_c}(\mathbf{P}) = \mathbf{K}_\mathrm{p}\mathbf{e} + \mathbf{K}_\mathrm{d}\dot{\mathbf{e}}. \tag{9}$$

where $\mathbf{F_c}(\mathbf{P}) \in \mathbb{R}^{3\times 1}$ is the controlled magnetic force. Realization of the controlled magnetic force is done using the inverse of the magnetic force-current map (8), by setting $\mathbf{F_c}(\mathbf{P})$ to $\mathbf{F}(\mathbf{P})$. In (9), $\mathbf{K_p} \in \mathbb{R}^{3\times 3}$ and $\mathbf{K_d} \in \mathbb{R}^{3\times 3}$ are the controller positive-definite gain matrices. Further, $\mathbf{e} \in \mathbb{R}^{3\times 1}$ and $\dot{\mathbf{e}} \in \mathbb{R}^{3\times 1}$ are the position and velocity tracking errors, respectively, and are given by

$$\mathbf{e} = \mathbf{P} - \mathbf{P_{ref}} \quad \text{and} \quad \dot{\mathbf{e}} = \dot{\mathbf{P}} - \dot{\mathbf{P}}_\mathbf{ref} = \dot{\mathbf{P}}. \tag{10}$$

Substituting (9) into the force equation (1) yields the following error dynamics:

$$\dot{\mathbf{e}} + \left(\mathbf{K_d} + \gamma\mathbf{\Pi}\right)^{-1}\mathbf{K_p}\mathbf{e} = -\left(\mathbf{K_d} + \gamma\mathbf{\Pi}\right)^{-1}\mathbf{K_p} f\hat{\mathbf{u}}, \tag{11}$$

where $\hat{\mathbf{u}}$ is a unit vector of the self-propulsion force of our microrobots. Further, $\mathbf{\Pi} \in \mathbb{R}^{3\times 3}$ is the identity matrix. The error dynamics (11), indicates that the matrix $\left(\left(\mathbf{K_d} + \gamma\mathbf{\Pi}\right)^{-1}\mathbf{K_p}\right)$ must be positive definite. The self-propulsion force can be overcome by increasing the gain matrix ($\mathbf{K_d}$), which in turn results in better positioning accuracy in the vicinity of the reference position. However, this increase necessitates the generation of relatively large magnetic field gradients that cannot be generated using our magnetic system (maximum magnetic field gradient is 60 mT/m). Nevertheless, selecting the entries of the matrices ($\mathbf{K_p}$ and $\mathbf{K_d}$) such that $\left(\mathbf{K_d} + \gamma\mathbf{\Pi}\right)^{-1}\mathbf{K_p}$ is positive definite, ensures that our microrobots are oriented towards a reference position. Due to the self-propulsion force (right-hand side of (11)), the tracking error cannot be zero.

We only consider the motion control of microrobots in a two-dimensional space, i.e., the center plane of our magnetic system. In this plane, the vertical components of our magnetic fields are zero. Further, the reference positions are fixed ($\dot{\mathbf{P}}_\mathbf{ref} = 0$).

A. Motion Control of Magnetotactic Bacteria

Motion control of an MTB is implemented inside a capillary tube with growth medium. The *Magnetospirillum magnetotacticum* MS-1 culture utilized in our experimental work is grown according to the protocol provided by Bertani *et al.* [18]. Our magnetotactic bacteria provide thrust force with an order of magnitude of 10^{-12} N using each of their flagella. This force is almost five orders of magnitude higher than the pulling magnetic force generated using our magnetic system (the average magnetic dipole moment is on the order of 10^{-17}). Therefore, our control strategy is based on using (9) just to position an MTB within the vicinity of a given reference position within a planar workspace of 300 μm $\times$ 200 μm, inside a capillary tube (Fig. 1). Fig. 4 shows a representative motion control result of an MTB using control law (9). In this experiment the MTB is positioned at a velocity of 30 μm/s. The control system positions the MTB within the vicinity of two reference positions with regions of convergence of 40 μm and 20 μm in diameter. This experiment is repeated 10 times using different magnetotactic bacteria from the same culture. The

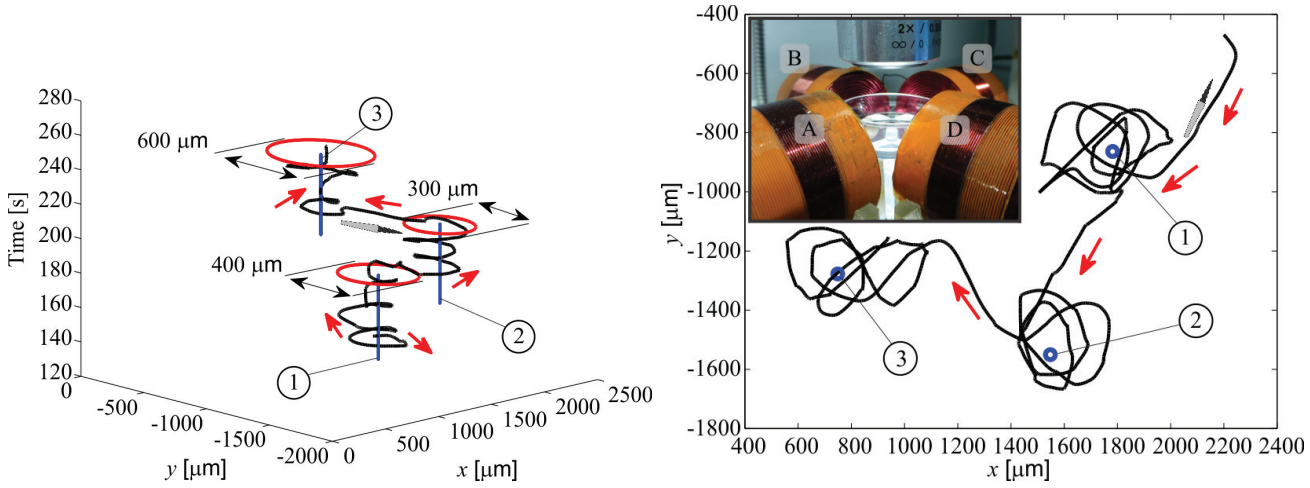

(a) Path of the controlled microjet

(b) Microjet within the vicinity of three reference positions

Fig. 5. Representative closed-loop motion control result of a microjet under the influence of the controlled magnetic fields. Our microjet is positioned within the vicinity of three reference positions using control law (9). The entries of the diagonal matrices $\mathbf{K}_{\mathrm{p}}$ and $\mathbf{K}_{\mathrm{d}}$ are 15 s^{-2} and 15.5 s^{-1}, respectively. (a) A microjet is controlled at an average velocity of 90 μm/s. The control system positions the microjet within the vicinity of three reference positions (vertical blue lines) with regions of convergence of 400 μm, 300 μm and 600 μm in diameter. (b) The control system reverses the direction of the magnetic fields to position the microjet within the vicinity of the reference positions (blue circles), based on (11). The inset shows the array of electromagnets and the petri dish which contains the microjets. *Please refer to the attached video that demonstrates the results of the closed-loop control of the self-propelled microjet.*

average velocity and average region of convergence are 32 μm/s and 23 μm, respectively. *Please refer to the attached video that demonstrates a representative result of the closed-loop control of an MTB.*

B. Motion Control of Microjets

Motion control of microjets is implemented inside a petri dish with hydrogen peroxide solution, shown in the inset of Fig. 5(b). The petri dish contains 1 ml of hydrogen peroxide solution and Triton X at concentrations of 5% and 5%, respectively. The catalytic reaction between the hydrogen peroxide solution and the platinum layers of the microjet is observed after the addition of 100 μl of hydrogen peroxide solution at concentration of 15%. Similar to magnetotactic bacteria, microjets provide thrust force that cannot be overcome using the maximum magnetic field gradient generated by our magnetic system. Therefore, our control system only positions the microjet within the vicinity of the reference position. Fig. 5 shows a representative motion control result of a microjet. Three reference positions are tracked at a velocity of 90 μm/s. The control system positions the microjet within regions of convergence of 400 μm, 300 μm and 600 μm in diameter. This motion control experiment is repeated 10 times using different microjets. The average velocity and average region of convergence are 119 μm/s and 417 μm, respectively. *Please refer to the attached video that demonstrates a representative result of the closed-loop control of a self-propelled microjet.*

C. Magnetotactic Bacteria Versus Microjets

Magnetotactic bacteria and microjets have a similar propulsion mechanism. Both microrobots navigate in a low Reynolds number regime by converting the chemical energy into kinetic energy. Magnetotactic bacteria provide propulsion by their flagella, whereas microjets provide propulsion by the thrust force generated using the ejecting oxygen bubbles from one of their ends (Fig. 1 and Fig. 2). These self-propulsion forces allow magnetotactic bacteria and microjets to overcome drag forces of 3.8×10^{-16} N at 32 μm/s and 1.4×10^{-14} N at 119 μm/s (drag forces are calculated using (3)), respectively. Further, the self-propulsion forces allow our magnetotactic bacteria and microjets to have average velocities of 6 and 2 body lengths per second, respectively.

The characterized average magnetic dipole moments of our magnetotactic bacteria and microjets are 1.4×10^{-17} A.m^2 and 1.5×10^{-13} A.m^2, respectively. These magnetic dipole moments are due to the magnetite nanocrystals (Fig. 2) and magnetic layers of the magnetotactic bacteria and microjets, respectively. The self-propelled microrobots use these magnetic dipole moments to generate magnetic torque and align along the external magnetic field lines. Magnetotactic bacteria and microjets overcome maximum rotational drag torques of 2.9×10^{-20} N.m and 3.0×10^{-16} N.m (drag torques are calculated using (3)), respectively. Our control system does not have influence on the linear velocities of the magnetotactic bacteria and the microjets. This is due to the difference between the maximum magnetic force which can be generated using our magnetic system and the propulsion forces generated by the microrobots. Magnetotactic bacteria are positioned within the vicinity of reference positions at an average velocity of 32 μm/s, whereas microjets are positioned at an average velocity of 119 μm/s. Further, magnetotactic bacteria are positioned within an average region of convergence of 23 μm, while microjets are positioned within an average region of convergence of 417 μm in diameter, respectively.

TABLE I

MORPHOLOGICAL, FLUIDIC, MAGNETIC AND CONTROL CHARACTERISTICS OF MAGNETOTACTIC BACTERIA AND MICROJETS. AVERAGE IS CALCULATED FROM 15 SCANNING AND TRANSMISSION ELECTRON MICROSCOPY IMAGES FOR MAGNETOTACTIC BACTERIA, AND 10 CHARACTERIZATION AND CLOSED-LOOP MOTION CONTROL TRIALS FOR EACH MICROROBOT. THE DRAG COEFFICIENTS AND MAGNETIC DIPOLE MOMENTS ARE CALCULATED USING (4), (5) AND (7). CONTROL EXPERIMENTS ARE DONE USING SIMILAR CONTROLLER GAINS USING (9). ROC DENOTES THE REGION OF CONVERGENCE.

Characteristics	**Magnetotactic bacteria**	**Microjets**
Length [μm]	5.2 ± 0.5	50
Diameter [μm]	0.5 ± 0.1	5
Linear drag [N.m^{-1}.s]	1.2×10^{-8}	1.2×10^{-7}
Rotational drag [N.m.s]	8.3×10^{-20}	7.5×10^{-17}
Boundary frequency [rad/s]	2.2 ± 1.5	25.1 ± 7.4
Dipole moment [A.m^2]	1.4×10^{-17}	1.5×10^{-13}
Average velocity [μm/s]	32 ± 10	119 ± 30
Average ROC [μm]	23 ± 10	417 ± 105

Table I summarizes the results of our comparative study between the characterized morphological, fluidic, magnetic and control properties of the self-propelled microrobots. The morphological characteristics are determined using 15 SEM and TEM images of the magnetotactic bacteria, and single SEM image of the microjet.

IV. CONCLUSIONS AND FUTURE WORK

This work provides a comparative study between magnetotactic bacteria and microjets. Fluidic properties in terms of linear and rotational drag coefficients are calculated for the microrobots based on their characterized morphologies and the properties of their growth medium and hydrogen peroxide solution. Based on the morphological and fluidic properties, the magnetic dipole moments of the microrobots are characterized using the *rotating field* technique. Finally, we utilize the characterized magnetic dipole moments in the realization of closed-loop control systems. These control systems are used to provide a comparison between our microrobots in the transient- and steady-states (average velocity and average region of convergence). Our comparative study shows that magnetotactic bacteria and microjet move at velocities of 6 and 2 body lengths per second, and can be positioned within regions of convergence of 4 and 8 body lengths within the vicinity of reference positions, respectively.

As part of future work, our magnetic system will be integrated with an ultrasound imaging modality. In addition, our system will be redesigned to control magnetotactic bacteria and microjets in the three-dimensional space. Motion control of magnetotactic bacteria and microjets in microfluidic channels with time-varying fluid flow will be implemented.

REFERENCES

[1] Y. F. Mei, G. Huang, A. A. Solovev, E. B. Urena, I. Monch, F. Ding, T. Reindl, R. K. Y. Fu, P. K. Chu, and O. G. Schmidt, "Versatile approach for integrative and functionalized tubes by strain engineering of nanomembranes on polymers," *Advanced Materials*, vol. 20, no. 21, pp. 4085-4090, November 2008.

[2] A. A. Solovev, Y. F. Mei, E. B. Urena, G. Huang, and O. G. Schmidt, "Catalytic microtubular jet engines self-propelled by accumulated gas bubbles," *Small*, vol. 5, no. 14, pp. 1688-1692, July 2009.

[3] S. Martel, O. Felfoul, J.-B. Mathieu, A. Chanu, S. Tamaz, M. Mohammadi, M. Mankiewicz, and N. Tabatabaei, "MRI-based medical nanorobotic platform for the control of magnetic nanoparticles and flagellated bacteria for target interventions in human capillaries," *The International Journal of Robotics Research*, vol. 28, no. 9, pp. 1169-1182, September 2009.

[4] I. S. M. Khalil, M. P. Pichel, L. Zondervan, L. Abelmann, and S. Misra, "Characterization and control of biological microrobots," in *Proceedings of the 13th International Symposium on Experimental Robotics-Springer Tracts in Advanced Robotics*, Springer Tracts in Advanced Robotics (STAR), vol. 88, pp. 617–631, 2013.

[5] I. S. M. Khalil, M. P. Pichel, L. Abelmann, and S. Misra, "Closed-loop control of magnetotactic bacteria," *The International Journal of Robotics Research*, vol. 32, no. 6, pp. 637-649, May 2013.

[6] B. J. Nelson, I. K. Kaliakatsos, and J. J. Abbott, "Microrobots for minimally invasive medicine," *Annual Review of Biomedical Engineering*, vol. 12, pp. 55-85, April 2010.

[7] M. P. Kummer, J. J. Abbott, B. E. Kartochvil, R. Borer, A. Sengul, and B. J. Nelson, "OctoMag: an electromagnetic system for 5-DOF wireless micromanipulation," *IEEE Transactions on Robotics*, vol. 26, no. 6, pp. 1006-1017, December 2010.

[8] S. Martel and M. Mohammadi, "Using a swarm of self-propelled natural microrobots in the form of flagellated bacteria to perform complex micro-assembly tasks," in *Proceedings of the IEEE International Conference on Robotics and Automation (ICRA)*, pp. 500-505, Alaska, USA, May 2010.

[9] A. A. Solovev, S. Sanchez, M. Pumera, Y. F. Mei, and O. G. Schmidt, "Magnetic Control of Tubular Catalytic Microbots for the Transport, Assembly, and Delivery of Micro-objects," *Advanced Functional Materials*, vol. 20, no. 15, pp. 2430-2435, August 2010.

[10] S. Sanchez, A. A. Solovev, S. Schulze, and O. G. Schmidt, "Controlled manipulation of multiple cells using catalytic microbots," *Chemical Communication*, vol. 47, pp. 698-700, 2011.

[11] S. Martel, "Controlled bacterial micro-actuation," in *Proceedings of the International Conference on Microtechnologies in Medicine and Biology*, pp. 89-92, Okinawa, Japan, May 2006.

[12] S. Martel, C. C. Tremblay, S. Ngakeng, and G. Langlois, "Controlled manipulation and actuation of micro-objects with magnetotactic bacteria," *Applied Physics Letters*, vol. 89, no. 23, 233904, 2006.

[13] D. H. Kim, P. S. S. Kim, A. A. Julius, and M. J. Kim, "Three-dimensional control of engineered motile cellular microrobots," in *Proceedings of the IEEE International Conference on Robotics and Automation (ICRA)*, pp. 721-726, Minnesota, USA, May 2012.

[14] M. S. Sakar, E. B. Steager, D. H. Kim, A. A. Julius, M. Kim, V. Kumar and G. J. Pappas, "Modeling, control and experimental characterization of microbiorobots," *The International Journal of Robotics Research*, vol. 30, no. 6, pp. 647-658, May 2011.

[15] I. S. M. Khalil, M. P. Pichel, O. S. Sukas, L. Abelmann, and S. Misra, "Control of magnetotactic bacterium in a micro-fabricated maze," in *Proceedings of the IEEE International Conference on Robotics and Automation (ICRA)*, pp. 5488-5493, Karlsruhe, Germany, May 2013.

[16] Y. F. Mei, A. A. Solovev, S. Sanchez, and O. G. Schmidt, "Rolled-up nanotech on polymers: from basic perception to self-propelled catalytic microengines," *Chemical Society Review*, vol. 40, no. 5, pp. 2109-2119, May 2011.

[17] S. Sanchez, A. A. Solovev, S. M. Harazim, and O. G. Schmidt, "Microrobots swimming in the flowing streams of microfluidic channels," *Journal of the American Chemical Society*, vol. 133, no. 4, pp. 701-703, February 2011.

[18] L. E. Bertani, J. Weko, K. V. Phillips, R. F. Gray, and J. L. Kirschvink, "Physical and genetic characterization of the genome of Magnetospirillum magnetotacticum, strain MS-1," *International Journal on Genes and Genomes*, vol. 264, pp. 257-263, January 2001.

[19] H. C. Berg, "Random walks in biology," *Princeton University Press*, Princeton, New Jersey, 1993.

[20] Y. R. Chemla, H. L. Grossman, T. S. Lee, J. Clarke, M. Adamkiewicz, and B. B. Buchanan, "A new study of bacterial motion: superconducting quantum interference device microscopy of magnetotactic bacteria," *Biophysical Journal*, vol. 76, pp. 3323-3330, June 1999.